 doi:10.20944/preprints202103.0608.v1

Article

A Novel Hybrid Monte Carlo Algorithm for Sampling Path Space

F. J. Pinski[1]*

[1] Department of Physics, University of Cincinnati, Cincinnati, Ohio 45221, USA; frank.pinski@uc.edu
* Correspondence: frank.pinski@uc.edu; Tel.: +1-513-432-8717

Abstract: To sample from complex, high-dimensional distributions, one may choose algorithms based on the Hybrid Monte Carlo (HMC) method. HMC-based algorithms generate nonlocal moves alleviating diffusive behavior. Here, I build on an already defined HMC framework, Hybrid Monte Carlo on Hilbert spaces [A. Beskos, F.J. Pinski, J.-M. Sanz-Serna and A.M. Stuart, Stoch. Proc. Applic. 121, 2201 - 2230 (2011); doi:10.1016/j.spa.2011.06.003] that provides finite-dimensional approximations of measures π which have density with respect to a Gaussian measure on an infinite-dimensional Hilbert (path) space. In all HMC algorithms, one has some freedom to choose the mass operator. The novel feature of the algorithm described in this article lies in the choice of this operator. This new choice defines a Markov Chain Monte Carlo (MCMC) method which is well defined on the Hilbert space itself. As before, the algorithm described herein uses an enlarged phase space Π having the target π as a marginal, together with a Hamiltonian flow that preserves Π. In the previous method, the phase space π was augmented with Brownian bridges. With the new choice for the mass operator, π is augmented with Ornstein-Uhlenbeck (OU) bridges. The covariance of Brownian bridges grows with its length, which has negative effects on the Metropolis-Hasting acceptance rate. This contrasts with the covariance of OU bridges which is independent of the path length. The ingredients of the new algorithm include the definition of the mass operator, the equations for the Hamiltonian flow, the (approximate) numerical integration of the evolution equations, and finally the Metropolis-Hastings acceptance rule. Taken together, these constitute a robust method for sampling the target distribution in an almost dimension-free manner. The behavior of this novel algorithm is demonstrated by computer experiments for a particle moving in two dimensions, between two free-energy basins separated by an entropic barrier.

Keywords: Brownian Dynamics; Stochastic Processes; Sampling path space, transition paths

1. Introduction

Often it is important to understand how molecules change conformations. For example, the folding of proteins is of high interest[1], One approach is to simulate such transitions for generating a thermodynamic-relevant ensemble of paths that start in one free-energy basin and end in another. Underlying such paths is a model for dynamics. Here, the particles are assumed to undergo Brownian dynamics and are in contact with a thermal reservoir with the fixed temperature ε.

The Brownian dynamics providing the evolution of the particle position x is described by a Stochastic Differential Equation (SDE):

$$dx_t = F(x)\,dt + \sqrt{2\varepsilon}\,dW_t \tag{1}$$

where dW_t is the standard Weiner process. Here the force (drift) is assumed to be the (negative) gradient of a potential energy function $U(x)$, namely $F(x) = -\partial U/\partial x$.

By integrating the SDE forward in time, one assembles a trajectory: the starting position may be known, but not the ending point. As shown by Onsager and Machlup[2], the path probability can be expressed in terms of the path positions. The (negative) logarithm of this probability as become known as the Onsager-Machlup (OM) functional. As shown in Appendix A, the form of the functional depends of how the SDE (Equation 1) is discretized. To understand molecular transitions, it would be useful to extract a thermodynamic distribution of

Preprints (www.preprints.org) | NOT PEER-REVIEWED | Posted: 24 March 2021 doi:10.20944/preprints202103.0608.v1

paths that start in one free energy basin and end in another. For such constrained paths, an effective Hamiltonian can be formed and expressed as

$$H_{eff} = \frac{1}{2}\langle x\,|L|\,x\rangle + \Phi(x), \tag{2}$$

with the details given in Appendix A. Using this effective Hamiltonian, standard techniques can be used to sample the probability distribution at an effective temperature $\varepsilon_{eff} = 2\varepsilon/\Delta t$, with ε being the actual temperature and Δt is the time discretization step used in approximating the SDE.

Performing such path sampling is challenging for several reasons. Firstly as the time step used to solve the SDE becomes small, that is as $\Delta t \to 0$, contributions from the high frequency modes lead to divergence when evaluated using the effective Hamiltonian (Equation 2). Secondly, at each point along the path one must have a full description of the molecule. Thirdly, barriers separating different pathways may be insurmountable. Thus it is extremely important to have efficient algorithms to probe thermodynamic-relevant distribution of paths. The work by Beskos et al.[3] addresses the first of these issues using a Hybrid Monte Carlo[4] (HMC) method that augments path space with Brownian Bridges. One of the advantages is that HMC generates nonlocal moves alleviating diffusive behavior that plagues other methods[5]. However, the velocities, that form the Brownian Bridge, grow with the (time) path length. This growth negatively affects the algorithm accuracy. As shown in Section 2, by creating velocities that from an Ornstein-Uhlenbeck[6] (OU) Bridge, one can eliminate this dependence on the path length, while treating the high-frequency modes accurately. In Section 2, the algorithm for the deterministic integration in the Molecular Dynamics (MD) step is described, as well the associated error in the effective energy. In Section 3, an example in two dimensions is described as well as how the algorithmic parameters are chosen. This is follow in Section 4 by the description of results for sampling paths that contain a transition from one basin to another. In Section 5, continuous-time limit of the OM functional is sampled. As found before[7,8], the form produces unphysical results. The paper ends with a short discussion of how this new algorithm can be used in calculations employing the Path Integral Molecular Dynamic method, and finally with some concluding remarks.

2. Time Evolution of the Hamiltonian

To sample the probability distribution, the effective Hamiltonian, Equation 2 is augmented by including a Gaussian distributed variables that can be identified as the momentum, with the aim of using a Hybrid (or Hamiltonian) Monte Carlo (HMC) method[5].The method is summarized as follows: first pick the augmented variables from its known distribution, use them to (approximately) evolve the Hamiltonian flow, and then accept or reject the evolved path using the Metropolis-Hastings criterion. The augmented Hamiltonian is given by

$$H = \frac{1}{2}\left\langle p\,\middle|\,(L+A_{ou}^2\mathbb{1})^{-1}\,\middle|\,p\right\rangle + \frac{1}{2}\langle q\,|L|\,q\rangle + \Phi(q) \tag{3}$$

with both q and p being bridges, i.e. paths that start and end at the origin. Define $x = q + l_t$ as the physical path with l_t being a term linear in time that allows x to have the starting point $x(0) = x_-$ and the ending point $x(T) = x_+$. Note that $\Phi(x) = \Phi(q + l_t)$ and will be denoted as $\Phi(q)$. The path l_t is given by the linear (in t) relationship: $l_t = x_- + t\,(x_+ - x_-)/T$. The path p is the momentum conjugate to the path q. It is useful to work with the following Hamiltonian:

$$H_\alpha = \frac{1}{2}\left\langle p\,\middle|\,M^{-1}\,\middle|\,p\right\rangle + \frac{1}{2}\langle q\,|M|\,q\rangle + \alpha\left(\Phi(q) - \frac{1}{2}\left\langle q\,\middle|\,A_{ou}^2\,\middle|\,q\right\rangle\right) \tag{4}$$

with $M = L + A_{ou}^2\mathbb{1}$. Note that with $\alpha = 1$ this Hamiltonian (Equation 4) has the term $\frac{1}{2}\left\langle q\,\middle|\,A_{ou}^2\,\middle|\,q\right\rangle$ added and then subtracted. This algebraic manipulation importantly simplifies the numerical procedure as will be shown below. The role (and value) of the parameter α will be addressed later.

It is convenient to work with the velocities v given by $v = M^{-1}p$. The velocities comprise a bridge being zero at both endpoints. When $A_{ou} = 0$, the velocities comprise a Brownian Bridge, with covariance (with $t \geq s$)

Preprints (www.preprints.org) | NOT PEER-REVIEWED | Posted: 24 March 2021 doi:10.20944/preprints202103.0608.v1

being $\mathbb{E}\,v_s\,v_t = s(1-t/T)$ where T is the length of the path. This gives $\mathbb{E}\,v_{T/2}^2 = T/4$ which grows with the (time) length of the path. In contrast, the covariance of an OU bridge is given by

$$\mathbb{E}\,v_s\,v_t = \frac{2\,\varepsilon}{A_{ou}}\frac{\sinh(A_{ou}s)\,\sinh(A_{ou}(T-t))}{\sinh(A_{ou}T)} \quad \text{with } t \geq s, \tag{5}$$

with ε being the temperture. At the midpoint of the OU bridge, $\mathbb{E}\,v_{T/2}^2 \approx \varepsilon/A_{ou}$ when $A_{ou}T \gg 2$, which is independent of the path length T. In Appendix B, the numerical procedure for constructing an OU bridge is described.

Defining ϕ in terms of Φ as $\phi(\mathbf{q}) = \partial\Phi/\partial\mathbf{q}$, the equations of motion are given by

$$\begin{pmatrix} \frac{dq}{dt} \\ M\frac{dv}{dt} \end{pmatrix} = \underbrace{\begin{pmatrix} v \\ -M\,q \end{pmatrix}}_{\text{A}} + \alpha \underbrace{\begin{pmatrix} 0 \\ A_{ou}^2\,q - \phi(q) \end{pmatrix}}_{\text{B}} \tag{6}$$

with the A and B grouping being used in the splitting implemented in the numerical algorithms. This method used is symplectic as it corresponds to a Trotter[9]-Strang[10] procedure.

2.1. Splitting: ABA

The details of the ABA-splitting is given in this section. The BAB-splitting is regelated to Appendices C and D. Schematically the integration can be viewed as pictured in Equation 7. The ABA procedure begins with the initial position and velocity (q_0, v_0), then during the time interval $h/2$, these evolve into (q_H, v_H) using Equations 8 and 9. Next is the so-called full step, where the velocity evolves over a time h changing to w_H using Equation 10. The final step takes (q_H, w_H) and transforms them to (q_1, v_1) during a time interval $h/2$ using Equations 11 and 12.

$$\begin{pmatrix} q_0 \\ v_0 \end{pmatrix} \xRightarrow[\textbf{Half Step}]{\mathbf{A}(\mathrm{h}/2)} \begin{pmatrix} q_H \\ v_H \end{pmatrix} \xRightarrow[\textbf{Full Step}]{\mathbf{B}(\mathrm{h})} \begin{pmatrix} q_H \\ w_H \end{pmatrix} \xRightarrow[\textbf{Half Step}]{\mathbf{A}(\mathrm{h}/2)} \begin{pmatrix} q_1 \\ v_1 \end{pmatrix} \tag{7}$$

Half step, A: $\{q_0, v_0\} \Rightarrow \{q_H, v_H\}$ with $\theta = \frac{h}{2}$

$$\frac{dq}{dt} = v \quad \Rightarrow \quad q_H = \cos(\theta)\,q_0 + \sin(\theta)\,v_0 \tag{8}$$

$$\frac{dv}{dt} = -q \quad \Rightarrow \quad v_H = -\sin(\theta)\,q_0 + \cos(\theta)\,v_0 \tag{9}$$

Full step, B: $\{q_H, v_H\} \Rightarrow \{q_H, w_H\}$ with $M = (L + A_{ou}^2\mathbb{1})$

$$M\frac{dv}{dt} = -\alpha\,(\phi(q) - A_{ou}^2 q) \;\Rightarrow M(\Delta\overline{v}) = -\alpha\,h\,(\phi(q_H) - A_{ou}^2 q_H) \tag{10}$$

with $\Delta\overline{v} = w_H - v_H$.

Half step, A: $\{q_H, w_H\} \Rightarrow \{q_1, v_1\}$ with $\theta = \frac{h}{2}$

$$\frac{dq}{dt} = v \quad \Rightarrow \quad q_1 = \cos(\theta)\,q_H + \sin(\theta)\,w_H \tag{11}$$

$$\frac{dv}{dt} = -q \quad \Rightarrow \quad v_1 = -\sin(\theta)\,q_H + \cos(\theta)\,w_H \tag{12}$$

Note that the integrations in the half steps are exact, while the full step integration is approximate. As the numerical algorithm is based on a symmetric splitting of the time evolution operator, it is symplectic and represents the flow of a shadow Hamiltonian[11,12]. Thus for small integration time h, the energy error will be bounded. In the following section, we investigate the formula for this error.

Preprints (www.preprints.org) | NOT PEER-REVIEWED | Posted: 24 March 2021 doi:10.20944/preprints202103.0608.v1

2.2. "Energy" Error

The deterministic MD integration is preformed over a total time $N_{MD}\,h$. For each time increment, the integration corresponds to the ABA method described above. The total energy error for the MD integration can be determined from the sum of the errors of each ABA step. The it is sufficient to find the expression for the energy error in a single ABA step.

The error of the "energy" in the ABA step is due to the middle (full) step B, since the first and third steps reflect exact integrations. The error is given by

$$\begin{aligned}\Delta E^{(01)} \quad &= \Phi(q_1) - \Phi(q_0) - \frac{1}{2}\langle q_1 \,|A_{ou}^2|\, q_1\rangle + \frac{1}{2}\langle q_1 \,|A_{ou}^2|\, q_0\rangle \\ &+ \frac{1}{2}\langle v_1 \,|M|\, v1\rangle - \frac{1}{2}\langle v_0 \,|M|\, v_0\rangle + \frac{1}{2}\langle q_1 \,|M|\, q1\rangle - \frac{1}{2}\langle q_0 \,|M|\, q_0\rangle \end{aligned} \tag{13}$$

which simplifies to

$$\Delta E^{(01)} = \Phi(q_1) - \Phi(q_0) - \frac{1}{2}\langle q_1 + q_0 \,|A_{ou}^2|\, q_1 - q_0\rangle + \frac{1}{2}\langle w_H + v_H \,|M|\, w_H - v_h\rangle\,. \tag{14}$$

Substituting for v_H and w_H, one transforms the last term using

$$\langle w_H + v_H \,|M|\, w_H - v_h\rangle = -\frac{h\,\alpha}{\sin\theta}\left\langle \phi(q_h) - A_{ou}^2 q_H \,\middle|\, q_1 - q_0 \right\rangle \tag{15}$$

The value of α can be chosen to be $\alpha = \mathrm{sinc}\,(h/2)$. With this value of α, the energy error is given as

$$\Delta E^{(01)} = \Phi(q_1) - \Phi(q_0) \;\; - \left\langle \phi(q_H) - A_{ou}^2\left(q_h - \overline{q}_{01}\right) \,\middle|\, q_1 - q_0 \right\rangle \tag{16}$$

with $\overline{q}_{01} = (q_1 + q_0)/2$. Now it is clear why α was chosen in this way. The approximate equations of motion reproduce the flow of a shadow Hamiltonian [11,12]. The flow produced by numerically solving the equations of motion with $\alpha = \mathrm{sinc}\,(h/2)$ is evidently closer to the actual flow than using unit α.

The full step in the ABA splitting is

$$M\,\Delta v = -\alpha\, h\,(\phi(q_H) - A_{ou}^2 q_H) \tag{17}$$

The operator M^{-1} is defined with the boundary conditions such that Δv is zero at both the beginning and end of the path. The above equation is then a matrix equation:

$$\mathbb{M}\,\Delta v = \mathbf{b} \tag{18}$$

with $\mathbb{M}$ being a symmetric real tridiagonal matrix, with the only nonzero elements given by

$$\mathbb{M}_{i,i} = A_{ou}^2 + \frac{2}{\Delta t^2} \qquad\qquad \mathbb{M}_{i,i+1} = \mathbb{M}_{i+1,i} = -\frac{1}{\Delta t^2}. \tag{19}$$

With the vanishing of Δv at both ends of the path, there are no endpoint corrections to $\mathbb{M}$. To solve the matrix equation, the standard Gaussian elimination procedure is used (without pivoting).

3. Numerical Experiments

To explore the efficacy of the HMC method described above, I chose a two-dimensional example. A particle moves in a potential is given by

$$U\,(x,y) \;=\; \exp\Big(\; -2\left(x + \frac{1}{2}\right)^2 - 3\,(y+1)^2 \;\Big) + \left(x^2 + y^{16} - 1\right)^2 \tag{20}$$

Preprints (www.preprints.org) | NOT PEER-REVIEWED | Posted: 24 March 2021 doi:10.20944/preprints202103.0608.v1

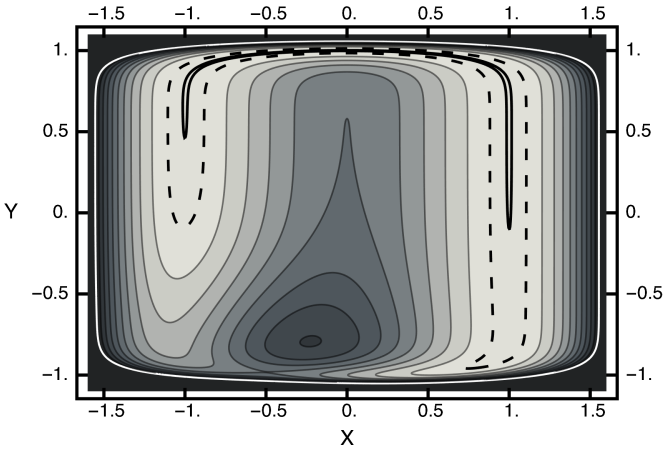

Figure 1. Contour plot of the two-dimensional potential. The horizontal axis corresponds to the x value; the vertical axis, the y axis. The value of the white contour is 2, of the dashed contour is 0.05. The solid black contour enclosed by the dashed contour has a value of 0.001. The potential at the saddle point is approximately unity. The potential at the local maximum is ≈ 1.6.

where x and y are the usual Cartesian coordinates. The first term above is a unit Gaussian centered at $x_g = -0.5$ and $y_g = -1$. The second term is a trough, with minimum zero and somewhat squarish in shape. A contour plot of this potential is given in Fig. 1. In this figure note that the white contour corresponds to $U(x, y) = 2$, the dashed line designates the countour $U[x, y) = 0.05$ which incloses the solid black contour $U(x, y) = 0.001$. A saddle point exists near $x_s \approx -0.5$ and $y_s \approx -1$ with $U[x_s, y_s) = 1$. A local maximum exists near $x_m \approx -0.225$ and $y_m \approx -0.794$ with $U(x_m, y_m) \approx 1.6$. An energy-barrier-free channel exists connecting the two wells although it is severely narrow as it crosses the x-axis. Thus one can view this potential as consisting of two wells separated by an entropic barrier if the temperature is not too high. A temperature $\varepsilon = 0.05$ was used in the simulations reported on below.

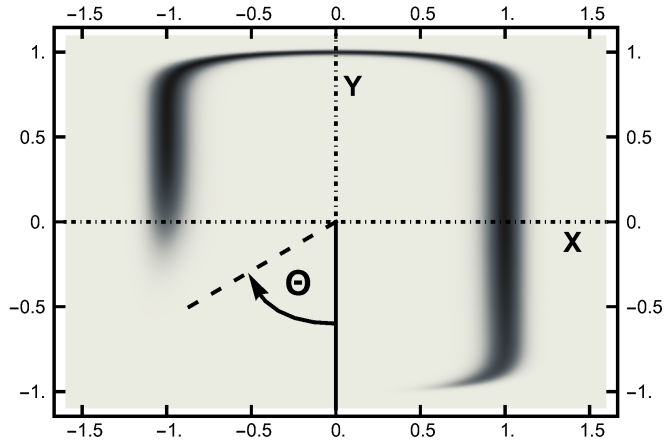

Figure 2. The equilibrium (Boltzmann) distribution for a temperature $\varepsilon = 0.05$ plotted as "density" plot. The black areas denote the higher probability areas, The narrow channel connects the left and right probability basins. The lack of an energy barrier is seen by the lack of variation in the shading along the channel. The angle Θ is pictured here.

3.1. Equilibrium distribution

The temperature $\varepsilon = 0.05$ is much smaller than the lowest energy barrier which is unity at the saddle point. The equilibrium (Boltzmann) distribution is displayed in the next two figures. In Figure 2, this distribution is shown in terms of a density plot. The narrow channel at the top of the figure connects the smaller basin on the

Preprints (www.preprints.org) | NOT PEER-REVIEWED | Posted: 24 March 2021 doi:10.20944/preprints202103.0608.v1

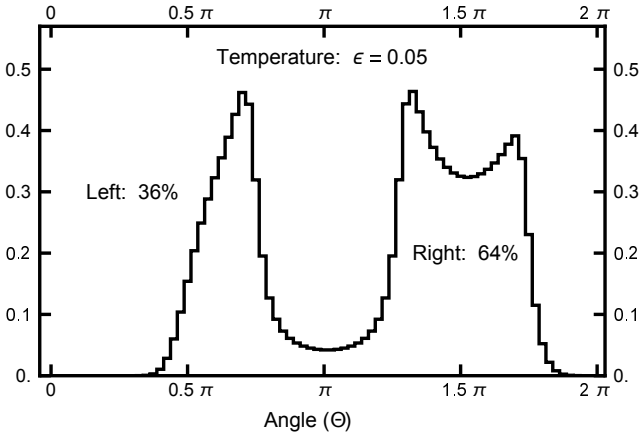

Figure 3. The function $\overline{P}(\Theta)$ plotted as a function of the angle Θ. See equation 21 for its definition. The value of $\delta = \pi/40$ was used. Notice that the single-peak structure on the left differs from the twin peaks on the right. This structure is caused the geometric factors which arise when the radius line slices the distribution function.

left with the larger basin (on the right). The lack of an energy barrier is reflected in the (equal) values of the distribution along the channel.

To quantify the equilibrium distribution, consider it as a function of the angle Θ which is defined in clockwise sense, measured with respect to the negative y axis, as shown in Figure 2. At a temperature $\varepsilon = 0.05$, the left basin has 36% of the weight, and the remaining 64% in the right basin. Defining $\overline{P}$ is given by

$$\overline{P}(\Theta) = (Z\,\delta)^{-1}\int_{\Theta-\delta/2}^{\Theta+\delta/2} d\theta \int_0^\infty r\,dr \exp\left(-\frac{U(-r\sin\theta, r\cos\theta)}{\varepsilon}\right). \tag{21}$$

In figure 3, $\overline{P}$ is plotted to emphasize the entropic barrier between the two basins. Remember that the potential is almost vanishing in the connecting channel.

3.2. Parameter Tuning

Unless stated otherwise, the form of the OM functional used was that corresponding to the midpoint integration of the SDE as written in Equation A8. To investigate the 2-dimensional paths that contain a transition between the two basins, several parameters must be chosen; two are physical: the temperature and the path length. For this problem the temperature is chosen to be $\varepsilon = 0.05$ which is small compared to the unit energy barrier. Thus at this temperature, the narrowness of the channel will be the limiting factor in impeding basin hopping. The path length T must not be too long nor too short. For very short times, the motion will become ballistic and uninteresting. For very large T the path will be dominated by intra-basin motion which is not the focus of the study. The remaining parameters of those of the model: the integration time in the determinist integration, The OU Bridge parameters: A^x_{ou} and A^y_{ou}. And finally the value of the algorithmic time step h which will be determined by requiring the Metropolis-Hastings acceptance rate to be sufficiently large.

3.2.1. Path Length

The next point to address is how often the particle moves from one basin to another. To make an estimate of this transition time, I collected information from 10,000 realizations of Brownian dynamics by performing forward integrations of the two-dimensional SDE. Each integration started at the same place in the left basin. The results for the number of attempts residing in the right basin are tabulated as a function of integration time are plotted in figure 4. As one sees, the curve approaches its equilibrium value as the total time reaches 1000. When the elapsed time is ≈ 125, over a third of the realizations are in the right basin. Thus this latter value is what is chosen as a reasonable time (path length) for exploring doubly constrained paths when a transition occurs.

Preprints (www.preprints.org) | NOT PEER-REVIEWED | Posted: 24 March 2021 doi:10.20944/preprints202103.0608.v1

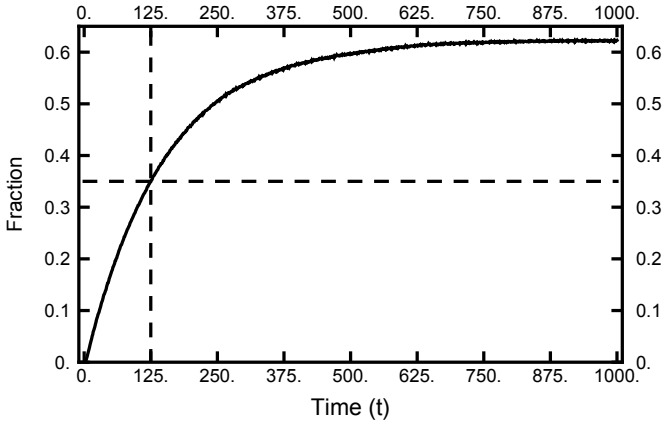

Figure 4. The results of 10,000 forward integrations of Brownian dynamics with temperature $\varepsilon = 0.05$. All had the same initial conditions (in the left basin). The plot gives the fraction of paths with positive values of x as a function of time. As the dotted lines indicate, after $T = 125$ over 35% of the integrations have ending points in the right well. As the integration time exceeds 1000, the fraction approaches the equilibrium distribution.

In the following sections, paths are examined that start in the left basin and end in the right basin, while time $T = 125$ has elapsed. The path is then described by 125,001 ordered pairs with $\Delta t = 1.0 \times 10^{-3}$.

3.2.2. Deterministic Integration Time

One of the advantages of the HMC method is its ability to generate nonlocal moves. This nonlocality of a proposed move can be described by a correlation function $d^{(x)}(nh)$, defined by

$$d^{(x)}(nh) = \sqrt{\sum_{i=1}^{N_t} \Big(x(nh) - x(0)\Big)^2 / N_t} \tag{22}$$

with a similar definition for $d^{(y)}(nh)$, where n is the number of the Molecular-Dynamics steps, and N_t is the number of points along the path. In Figure 5, $d^{(x)}(\tau)$ and $d^{(y)}(\tau)$ are plotted as functions of Molecular Dynamics integration time τ for two cases, 1.) $A_{ou}^{(x)} = A_{ou}^{(y)} = 0$ and 2.) $A_{ou}^{(x)} = A_{ou}^{(y)} = 1$. The time step parameter h was adjusted so that the (energy) errors were comparable, as seen in Figure 6. Such energy errors will be examined more closely later in the paper. As seen in Figure 5, both $d^{(x)}(\tau)$ and $d^{(y)}(\tau)$ level out for $\tau > 2$. Thus the MD integration time should be on the order of $\pi/2$ to balance the nonlocality of a proposed move with the required computational effort.. To avoid any resonances that might occur if a fixed integration time should be chosen, the (time) length of the integration is chosen to be uniformly distributed in the interval $(\pi/4, 3\pi/4)$ designated by the gray shaded area in Figure 5.]]

3.2.3. OU Bridge parameter $A_{ou}^{(x,y)}$

To understand how the choice of the A_{ou}^{x} and A_{ou}^{y} affect the sampling behavior, consider the plots of the correlation functions displayed in Figure 7. As shown in the this figure and in Figure 5, the y-degree of freedom shows the floppiness that corresponds the small energy cost of movement in that direction, on either the left or right basins. The relative stiffness of motion in the x direction is a direct result of the restriction due to the narrow channel connecting the two basins. The floppiness (in the y-direction) can be stiffened by increasing the value of A_{ou}^{y}. For the chosen integration times (as designated as a gray rectangle in Figure 7, values A_{ou}^{y} between 4 and 8 put the correlation function $d^{(y)}(\tau)$ in the same range as $d^{(x)}(\tau)$. However, decreasing A_{ou}^{x} below unity (not show in the figures) does not alter the stiffness in thel x-variable as its origin in due to the narrowness of the connecting channel.

Preprints (www.preprints.org) | NOT PEER-REVIEWED | Posted: 24 March 2021 doi:10.20944/preprints202103.0608.v1

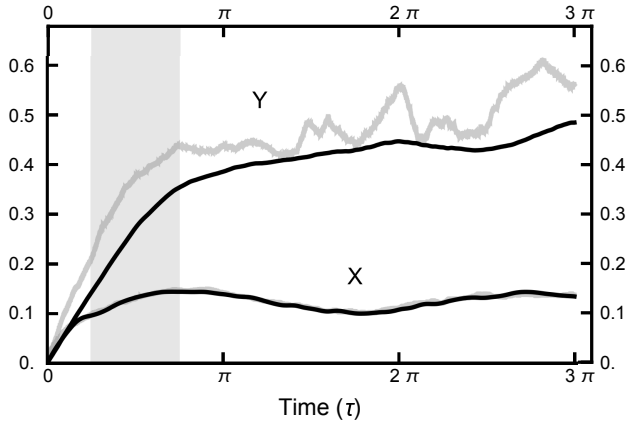

Figure 5. The correlation functions $d^{(x)}(\tau)$ and $d^{(y)}(\tau)$ for two runs. For the black curves, the parameters were $A^x_{OU} = A^y_{OU} = 1$; for the grays curves, $A^x_{OU} = A^y_{OU} = 0$. The black curve for $d^{(x)}(\tau)$ lies on top the gray curve.

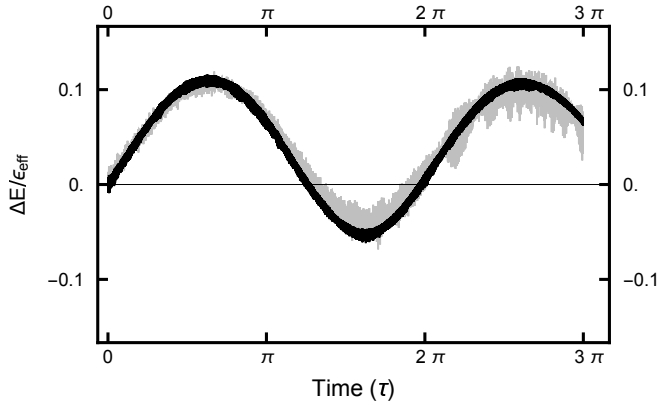

Figure 6. The energy error plotted as a function of MD integration time. The black curves designates the error for the case $A^{(x)}_{ou} = A^{(y)}_{ou} = 1$; the gray curves for $A^{(x)}_{ou} = A^{(y)}_{ou} = 0$. The time step parameter for the former case is $h = 6.667 \times 10^{-4}$ and for the latter $h = 6.667 \times 10^{-5}$. In the latter case, the smaller h meant that an order of magnitude more computing resources were required to generated the gray curves, as compared to the black ones. The top two curves show the behavior of $d^{(y)}(\tau)$. The curves for $d^{(x)}(\tau)$ almost lie on top of one another.

3.2.4. Time Step Size (h)

For the deterministic integration in the Molecular Dynamics (MD) step, a choice must be made for the size of the time step h. Since the numerical algorithm is based on a Trotter[9]-Strang[10] splitting, for small values of h, the energy error is bounded, as the energy of a "nearby" Hamiltonian, the Shadow Hamiltonian, is conserved. As shown in Figure 8, the energy error oscillates as a function of integration time τ. In addition, because of the stochastic nature of the integrals, the curves are noisy, with the noise increasing as h increases.

The choice for h is then determined by the Metropolis-Hastings acceptance rate. In Figure 9, this acceptance rate is plotted as a function of the time step h. As can be seen in the plot, the rate is a very steep function of h. Furthermore, when $A^x_{OU} = A^y_{OU} = 0$, $h < 0.0002$ to have a substantial acceptance rate, while when $A^x_{OU} = 1$ and $A^y_{OU} = 8$, h can be chosen almost two orders of magnitude larger. The dependence of the acceptance rate on the values of A^x_{OU} and A^y_{OU} show the power of the new algorithm presented here. A factor of 10 speedup can be obtained by choosing A^x_{OU} and A^y_{OU} to be unity. A larger speedup has been found with higher values of A^y_{OU}.

4. Path Sampling

As seen in Figures 2 and 3, in equilibrium a particle will spend a small fraction of time in the narrow channel. Thus the expectation is that a transition path would consist of motion in one basin or the other with a short transition while in the narrow channel. In the Figure 10, shows a typical path: it starts in in the left basin,

Preprints (www.preprints.org) | NOT PEER-REVIEWED | Posted: 24 March 2021 doi:10.20944/preprints202103.0608.v1

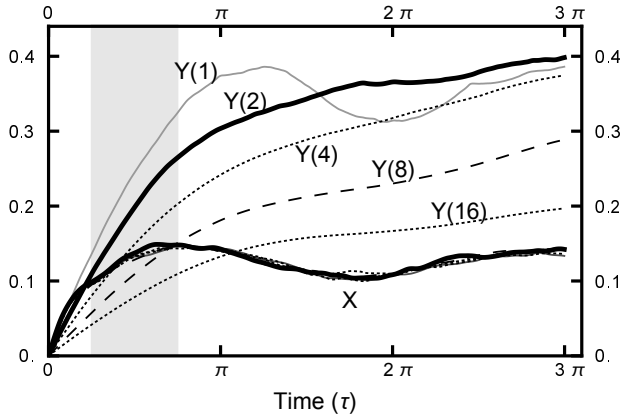

Figure 7. The correlation functions $d^{(x)}(\tau)$ and $A_{ou}^{(y)}$ for various runs. For all the runs $A_{ou}^{(x)} = 1$. From the top, the curves for $d^{(y)}(\tau)$ had the values of $A_{ou}^{(y)}$ of 1, 2, 4, 8 and 16 respectively. The curves for $d^{(x)}(\tau)$ lie on top of each other.

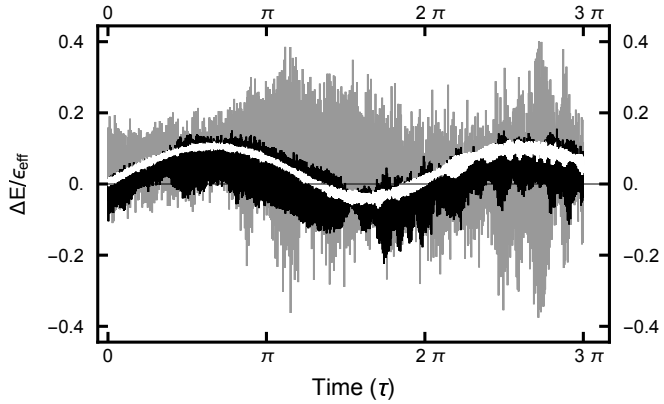

Figure 8. The effective-energy error plotted as a function of the MD integration time (τ). The three curves correspond to runs with values $A_{ou}^{(x)} = A_{ou}^{(y)} = 1$. The gray curve gives the error for the run with $h = 0.002$; the black curve, $h = 0.001$; and the white curve, $h = 0.00067$.

remaining in it for under 25% of the path length, making a transition, remaining in the right basin for the last 70% of the path. Because of the boundary conditions, at least one transition occurs. For the chosen path length of $T = 125.$, the simulations do not contain paths with more than a single transition. The shown path is the end result of a simulation using $A_{OU}^{x} = 1$ and $A_{OU}^{y} = 8$ and 100,000 Metropolis-Hastings steps.

In Figure 11, a summary of the evolution of this simulation is plotted. For these values of A_{OU}, on average the particle spends about 70% of the time in the right basin. The variation of this value is only few percent over the course of the simulation run. In Figure 12, a similar plot is show for the parameters $A_{OU}^{x} = 1$ and $A_{OU}^{y} = 4$, and 200,000 Metropolis-Hastings steps, twice as long as shown in Figure 11. The pictures are similar, except that the mean times have shifted, and the variation is larger in the second plot. The smaller variation in the first plot seems to be due to the large value of A_{OU}^{y} which dampens the oscillations in the y-component. But both cases show that the free energy of the right basin is larger that of the left basin.

Now consider Figure 13 where the complete information for the second simulation run is summarized. Here the normalized histogram is plotted for the run with $A_{OU}^{x} = 1$ and $A_{OU}^{y} = 4$. Note that the comparison with the equilibrium histogram is quite close. This closeness indicates that the series of paths accurately probe the potential shape of each basin.

The results shown in Figures 11 and 12, used an initial path where the fraction spent in the left basin was less that the fraction spent in the right. This was chosen because the relative fractions were near what is expected from their equilibrium ratio. In the next calculation, the starting path had a value for the fraction spent in the

Preprints (www.preprints.org) | NOT PEER-REVIEWED | Posted: 24 March 2021 doi:10.20944/preprints202103.0608.v1

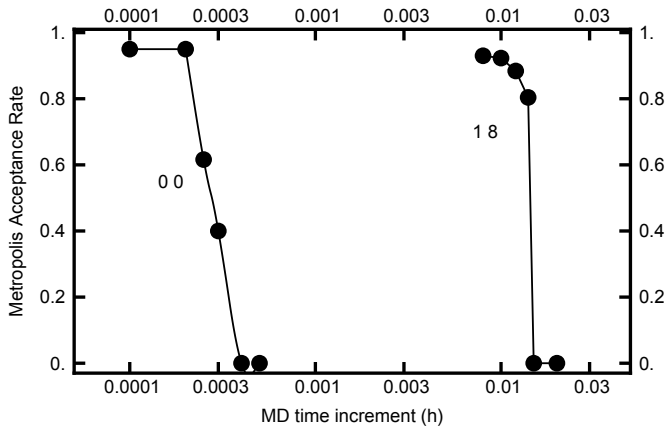

Figure 9. The Metropolis-Hastings acceptance rate for two runs. For the curve on the left, the parameters were $A^x_{OU} = A^y_{OU} = 0$, for the curve on the right, $A^x_{OU} = 1$ and $A^y_{OU} = 8$. For both runs, the number of Molecular Dynamics steps were chosen to be $(1+\eta)\pi/(4h)$ with η being a uniformly distributed random number in the unit interval.

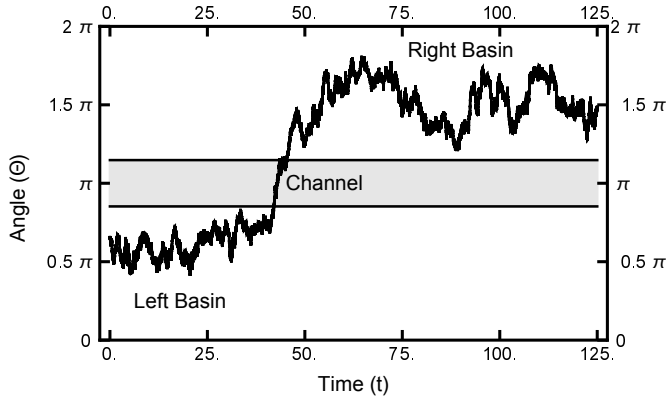

Figure 10. The one-dimensional representation of a typical path. The angle Θ plotted as a function of time. See figure 2 for the definition of Θ. At $t = 0$, the particle starts out in the left basin, makes its way through the narrow channel at $t \approx 50$ and ends in the right basin.

left well of $\approx 80\%$, very different from its equilibrium value. In Figure 14, the evolution of the right and left fractions are shown as a function of the algorithmic steps. In this simulation, $A^x_{OU} = A^y_{OU} = 1$ and MD time step was $h = 0.003$. As indicated, it took about $100,000$ steps before the left and right fractions became roughly equal, and twice that many steps before the right fraction became significantly larger that the left. The change in the fraction was due to the movement of the time at which the transition took place and not the creation of a new pair of transitions. One does see the incipient attempt at such a creation of a new pair of transitions at the $\approx$ 325000 step of the simulation. The attempt is evidence by the spike in the fraction of the path that is spent in the narrow channel, shown as the dark grey curve.

Preprints (www.preprints.org) | NOT PEER-REVIEWED | Posted: 24 March 2021 doi:10.20944/preprints202103.0608.v1

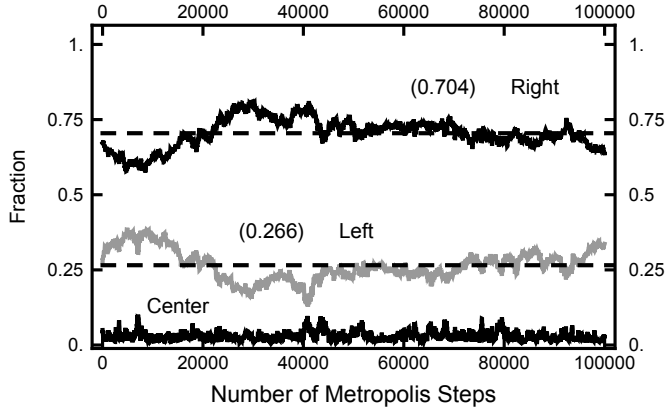

Figure 11. Results for a calculation with $A^x_{OU} = 1$ and $A^y_{OU} = 8$, The bottom (black) curve is the fraction of the path with $|x| < 1/2$; the middle (gray) curve is the fraction of the path with $x < -1/2$ and the top (black) curve is the fraction of the path with $x > 1/2$.

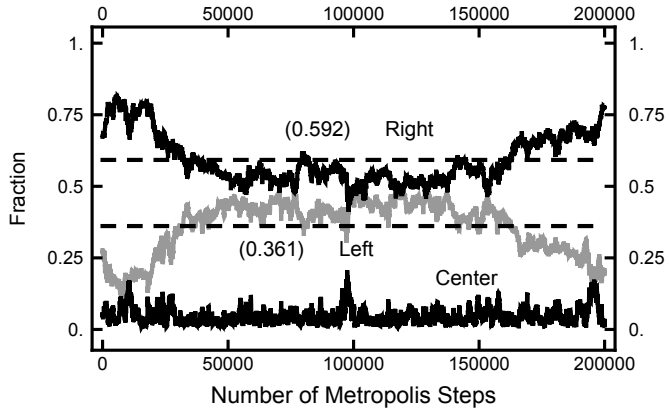

Figure 12. Results for a calculation with $A^x_{OU} = 1$ and $A^y_{OU} = 4$, The bottom (black) curve is the fraction of the path with $|x| < 1/2$; the middle (gray) curve is the fraction of the path with $x < -1/2$ and the top (black) curve is the fraction of the path with $x > 1/2$.

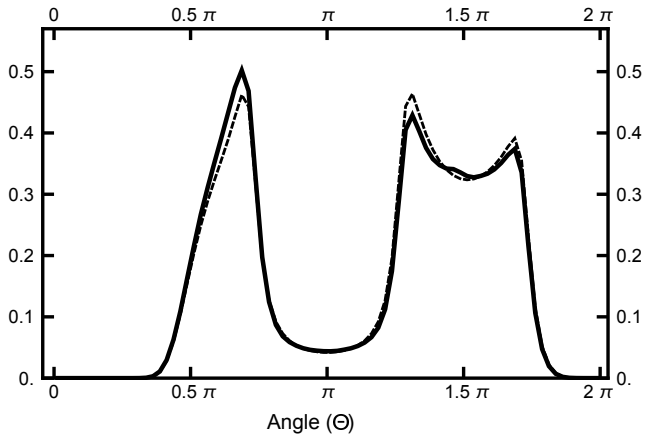

Figure 13. Results for a calculation with $A^x_{OU} = 1$ and $A^y_{OU} = 4$, The solid black curve is the histogram of the $\overline{P}(\Theta)$ for the 200,000 Metropolis steps pictured above in Figure 12. The dashed line represents the histogram that corresponds to the equilibrium distribution.

Preprints (www.preprints.org) | NOT PEER-REVIEWED | Posted: 24 March 2021 doi:10.20944/preprints202103.0608.v1

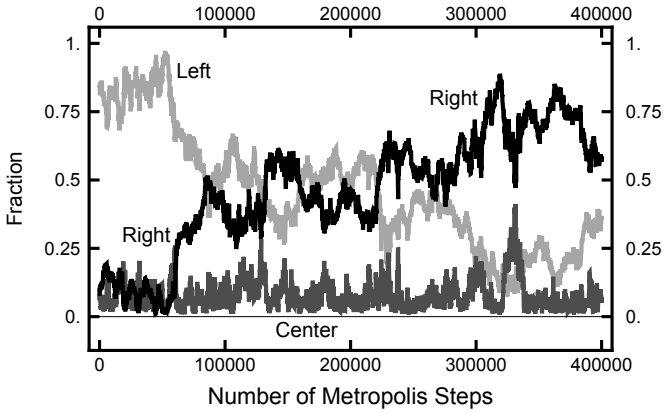

Figure 14. Results for a calculation with $A^x_{OU} = A^y_{OU} = 1$, The black curve is the fraction of the path with $x > 1/2$; the light gray curve is the fraction of the path with $x < -1/2$ and the bottom (dark gray) curve is the fraction of the path with $|x| < 1/2$.

Preprints (www.preprints.org) | NOT PEER-REVIEWED | Posted: 24 March 2021 doi:10.20944/preprints202103.0608.v1

5. Continuous-Time Limit

Now I turn to the calculations using the continuous-time limit of the OM functional[13,14]. The Radon-Nikodym derivative is manipulated using the Girsanov theorem and Ito's lemma. Displayed in Equation A10 this will denoted as the Ito-Girsanov measure. As shown in Figure 15, the results of a simulation using the Ito-Girsanov measure gives unphysical results. The paths converge very quickly to objects that look similar to noisy versions of the Most Probable Path (MPP), as shown in Figure 16. Notice that this behavior happens after only 5,000 hybrid steps. For calculations using the discrete form of the OM-function (Equation A4), a very different behavior is found as shown in Figure 11. The MPP reflects the maximum of the measure and is dominated by maxima of the Laplacian (of the physical potential). In the narrow channel, the Laplacian reflects the large curvature due to the confining sides. Similar to what was found before[7,8], the unphysical nature of these results were due to the buildup of correlations that are inconsistent with the assumption in the original SDE that the noise is white and uncorrelated with the particle position.

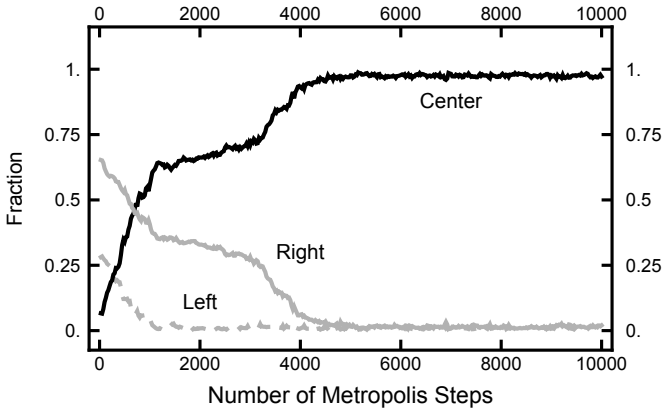

Figure 15. Results for a calculation with $A^x_{OU} = 1$ and $A^y_{OU} = 4$ using Equation A10 as the effective Hamilitonian, The black curve labeled Center is the fraction of the path with $|x| < 1/2$; the solid gray curve is the fraction of the path with $x > 1/2$ and the dashed gray curve is the fraction of the path with $x > 1/2$.

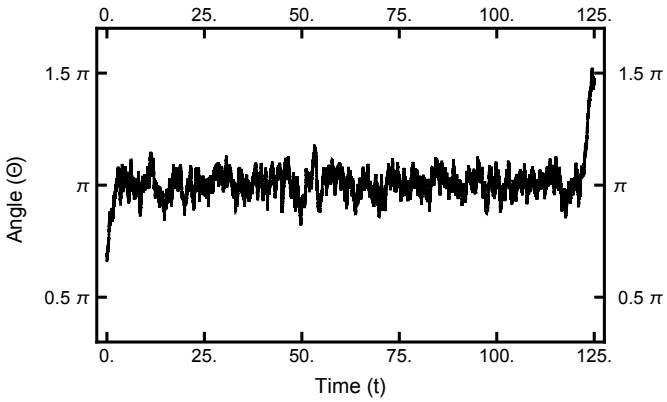

Figure 16. Results for a calculation with $A^x_{OU} = 1$ and $A^y_{OU} = 4$ using Equation A10 as the effective Hamilitonian, This is qualitatively different from the path plotted in Figure 10.

6. Discussion

The work reported here is relevant to that of Korol et al[15] who used a similar approach using path-integral molecular dynamics. In that work, the authors suggest that one should use mollified forces. This force mollification is a frequency dependent factor that limits the effects of high-frequency internal modes and yet keeps intact the low-frequency motion. In this current work, the mass operator is $M = L + A^2_{ou}\mathbb{1}$ performs this

Preprints (www.preprints.org) | NOT PEER-REVIEWED | Posted: 24 March 2021 doi:10.20944/preprints202103.0608.v1

task. Here A_{ou} can be adjusted to change the range for which the low frequencies are treated correctly. At high frequencies, the modes revert to the free-particle motion. This reversion is due to the effects of the L in the mass operator which dominates at high frequencies. The work described here then puts this "Force Mollification" into a consistent framework, incorporating the effects in a self-consistent manner.

If, instead of the dynamics, one is interested in highlighting particular modes, A_{ou} can be chosen differently for each mode. In particular, when working in normal mode coordinates, one can choose A_{ou} individually to minimize the size of Δv in Equation 10, thereby reducing the numerical errors in the integration.

7. Conclusion

A novel HMC procedure for sampling paths is presented here. This new procedure is much more efficient than previous methods, resulting in an order of magnitude speedup for the 2-dimensional problem explored. The novelty in the procedure lies in the choice of the mass matrix and concomitantly the velocities that form an OU Bridge. Using this new procedure, I successfully examined transition across an entropic barrier finding that the method can determine the relative free energy of the two basins that are not separated by an energy barrier.

Again, using the Ito-Girsanov measure has been found to give unphysical results. The sampling procedure, for the two-dimensional problem examined, converges to paths that look like noisy versions of the MPP[16] (most probable path), where the vast majority of the path is trapped in the narrow channel that connects the probability basins. It is clear that the large Laplacian (of the potential) is the dominant source of this unphysical feature.

The procedure is also useful for calculations using path-integral molecular dynamics[15] since the effective Hamiltonian has a similar form to that studied here. The novel procedure naturally folds the "mollification" of forces into the HMC formalism. This clearly shows the origins of this mollifying effect. that is, the mass matrix can reproduce the effect. The parameters $\{A_{ou}\}$in this method can be tuned for each degree of freedom, and they can be tuned differently to emphasize different physical effects. In addition, this method may be adapted to be used with the OBABO integration scheme[17] or with the second order Langevin method[18].

Acknowledgments: I wish to acknowledge many conversations with Patrick Malsom, Andrew Stuart, Kody Law, Gideon Simpson, and Robin Ball.

Author Contributions: The author solely formulated the ideas and performed the calculations presented in this paper.

Conflicts of Interest: The author declares that he does not have a conflict of interest.

Appendix A. Onsager-Machlup functionals

In this appendix, we delineate the algebraic forms of the OM functions. For simplicity the one-dimensional form of the equations are written down below; the multi-dimensional generalization is straight forward. First recognize that different discretizations of the SDE (Equation 1) result in different forms of the OM function[19] . Here two are considered: Euler-Maruyama and midpoint methods. The former is given by

$$x_{n+1} = x_n + F(x_n)\,\Delta t + \sqrt{2\,\varepsilon\,\Delta t}\;\xi_{n+1} \tag{A1}$$

where ξ_n is a random Gaussian variate with mean zero and unit variance and Δt is the time increment. The original Onsager-Machlup functional is based on this expression. If one iterates Equation A1 N_t times, one obtains a sequence of points $\{x_0, x_1, x_2, x_3, x_4, \ldots x_{n_t}\}$, with a probability

$$P_{EM} \;=\; (2\,\pi)^{-n_t/2} \prod_{n=1}^{n_t} \exp\Big(-\frac{1}{2}\xi_n^2\Big) \tag{A2}$$

Onsager and Machlup recognized that one can rewrite this probability distribution in terms of the path positions as $P_{EM} \propto \exp(-I_{OM})$ with

$$I_{OM} = \frac{\Delta t}{2\varepsilon} \sum_{n=1}^{n_t} \frac{1}{2}\left(\frac{x_{n+1}-x_n}{\Delta t} - F(x_n)\right)^2 \tag{A3}$$

Preprints (www.preprints.org) | NOT PEER-REVIEWED | Posted: 24 March 2021 doi:10.20944/preprints202103.0608.v1

Defining $\varepsilon_{eff} = 2\varepsilon/\Delta t$ as an effective temperature, the thermodynamic distribution is given in terms of P_{EM}, given by

$$P_{EM} \propto \exp\left(-\frac{H_{EM}}{\varepsilon_{eff}}\right)$$

with

$$H_{EM} = \sum_{n=1}^{n_t} \frac{1}{2}\left(\frac{x_{n+1}-x_n}{\Delta t}\right)^2 - \left(\frac{x_{n+1}-x_n}{\Delta t}\right) F(x_n) + \frac{1}{2}F(x_n)^2$$

which can be rewritten as

$$\begin{aligned} H_{EM} \quad &= \frac{1}{2\Delta t^2}\sum_{n=2}^{n_t-1} x_n\left(2x_n - x_{n+1} - x_{n-1}\right) \\ &+ \sum_{n=1}^{n_t}\left(\frac{1}{2}F(x_n)^2 - \left(\frac{x_{n+1}-x_n}{\Delta t}\right) F(x_n)\right) \end{aligned} \tag{A4}$$

With resumming, the first term was transformed:

$$\sum_{n=1}^{n_t} \frac{1}{2}\left(\frac{x_{n+1}-x_n}{\Delta t}\right)^2 = \frac{1}{2}\langle x|L|x\rangle$$

The last term in Equation A4 will be denoted as $\Phi_{EM}(\{x\})$ then the effective Hamiltonian can be written as

$$H_{EM} = \frac{1}{2}\langle x|L|x\rangle + \Phi_{EM}(\{x\}) \tag{A5}$$

Another discretiztion of the SDE (Equation 1) uses the midpoint and is written as

$$x_{n+1} = x_n + F(x_{mp})\,\Delta t + \sqrt{2\varepsilon\,\Delta t}\;\xi_{n+1} \tag{A6}$$

with $x_{mp} = (x_{n+1} + x_n)/2$. The effective Hamiltonian is a bit more complicated because of the Jacobian and again can be put in the form:

$$H_{mp} = \frac{1}{2}\langle x|L|x\rangle + \Phi_{mp}(\{x\}) \tag{A7}$$

where

$$\Phi_{mp}(\{x\}) = -\frac{2\varepsilon}{\Delta t}\sum_{n=1}^{n_t} \ln(\det J_n) + \sum_{n=1}^{n_t}\left(\frac{1}{2}F(x_{mp})^2 - \left(\frac{x_{n+1}-x_n}{\Delta t}\right) F(x_{mp})\right) \tag{A8}$$

where J_n is the Jacobian matrix whose elements are

$$J_{(\alpha,\beta)} \propto \delta_{\alpha,\beta} + \frac{\Delta t}{2}\frac{\partial^2 U}{\partial x_\alpha\,\partial x_\beta} \tag{A9}$$

and where the Jacobian J_n is evaluated at the midpoint.

And lastly, the continuous time limit of equations A5 and A7 can be written down as

$$H_{IG} = \frac{1}{2}\langle x|L|x\rangle + \Phi_{IG}(\{x\}) \tag{A10}$$

with

$$\Phi_{IG}(\{x\}) = \sum_{n=1}^{n_t} G(x_n)$$

Preprints (www.preprints.org) | NOT PEER-REVIEWED | Posted: 24 March 2021 doi:10.20944/preprints202103.0608.v1

where

$$G(x_n) = \frac{1}{2} F^2(x_n) - \varepsilon \, \Delta U \tag{A11}$$

with ΔU being the Laplacian of U.

Appendix B. Constructing Ornstein-Uhlenbeck (OU) Bridges

The following describes the method used to construct Ornstein-Uhlenbeck (OU) bridges. An OU bridge is an OU process that begins and ends at the origin. Consider the standard OU process for a variable Z_i given by the following SDE:

$$dZ_t = -A Z_t \, dt + \sqrt{2\varepsilon} \; dW_t \tag{A12}$$

with A being the OU parameter and ε being the temperature.

To form a realization of an OU process, we use the close relationship between HMC and Metropolis Adjusted Langevin Algorithm (MALA). To sample the Boltzmann distribution for a harmonic potential, the Hamiltonian is augmented by auxiliary variables which can be viewed as momenta, conjugate to the position variables. In one dimension this given by

$$H = \frac{1}{2} p^2 + \frac{1}{2} A x^2 \tag{A13}$$

The equations of motion are then

$$\frac{dx}{dt} = p \qquad \text{and} \qquad \frac{dp}{dt} = -A x \tag{A14}$$

The HMC procedure is first to form the momentum $p_0 = \sqrt{\varepsilon}\, \xi$ where ε is the temperature and ξ is a Gaussian random variate with mean zero and unit variance.

If one integrates the equations of motion over a time h and using the velocity-Verlet approximation, one obtains

$$x_1 = x_0 + p_0 \, h - \frac{A}{2} x_0 \, h^2 \tag{A15}$$

which becomes

$$x_1 - x_0 = -A \, x_0 \, \Delta t + \sqrt{2 \varepsilon \, \Delta t} \; \xi \tag{A16}$$

with $\Delta t = h^2/2$. This is then the Euler-Maruyama[20] formula for the OU process. Within the one-step HMC, one uses the Metropolis-Hastings step to accept or reject the proposed move

$$\{x_0, p_0\} \to \{x_1, p_1 = p_0 - \sqrt{\frac{\Delta t}{2}} \, A \, (x_0 + x_1)\}. \tag{A17}$$

Such a move may be rejected if the energy error is too large.

However, the equations of motion above can be integrated exactly which gives

$$x_1 = x_0 \cos \sqrt{2 A \, \Delta t} \; + \; \xi_i \sqrt{\frac{\varepsilon}{A}} \sin \sqrt{2 A \, \Delta t}. \tag{A18}$$

In such a method, no proposed moves will be rejected in the Metropolis-Hastings step. Thus we string such steps together using

$$x_{i+1} = x_1 \cos \sqrt{2 A \, \Delta t} \; + \; \xi_i \sqrt{\frac{\varepsilon}{A}} \sin \sqrt{2 A \, \Delta t}. \tag{A19}$$

To first order in Δt, the above agrees with other expressions for forming a realization of an OU process. The advantage of this above form is that for any size of Δt, the path asymptotically approaches the target Boltzmann distribution.

Now the ending point of the OU bridge needs to be addressed. The ending point of an OU bridge is also zero, but this is not the case for a typical realization of an OU process. To form a bridge, two OU processes

Preprints (www.preprints.org) | NOT PEER-REVIEWED | Posted: 24 March 2021 doi:10.20944/preprints202103.0608.v1

can be combined by the following procedure. Assume that $Z^{(1)}$ and $Z^{(2)}$ are two different finite realizations of equation A12; both starting at the origin with endpoints $z_N^{(1)}$ and $z_N^{(2)}$ respectively. The linear combinations

$$Z_{\pm}^{(3)} = \pm\left(Z^{(1)}\cos\kappa + Z^{(2)}\sin\kappa\right) \tag{A20}$$

are also realizations of the same OU process. Then the angle κ can be chosen by $\tan\kappa = -z_N^{(1)}/z_N^{(2)}$ which makes endpoints of $Z_{\pm}^{(3)}$ to be $z_N^{(3)} = 0$. With this choice of κ, the OU processes $Z_{\pm}^{(3)}$ are OU bridges. Other ways exist in the literature for forming OU bridges, see for example Barczy and Kern[21]. However I found them numerically unstable due to the need to calculate the ratios of sinhs with large arguments.

Appendix C. BAB Splitting: Numerical Integration

$$\begin{pmatrix} q_0 \\ v_0 \end{pmatrix} \xrightarrow[\text{Half Step}]{\mathbf{B}(h/2)} \begin{pmatrix} q_0 \\ v_H \end{pmatrix} \xrightarrow[\text{Full Step}]{\mathbf{A}(h)} \begin{pmatrix} q_1 \\ w_H \end{pmatrix} \xrightarrow[\text{Half Step}]{\mathbf{B}(h/2)} \begin{pmatrix} q_1 \\ v_1 \end{pmatrix} \tag{A21}$$

half step, B: $\{q_0, v_0\} \Rightarrow \{q_0, v_H\}$ with $M = (L + A_{ou}^2\mathbb{1})$

$$M\frac{dv}{dt} = -(\phi(q) - A_{ou}^2 q) \;\Rightarrow M\Delta v_0 = -\frac{h}{2}(\phi(q_0) - A_{ou}^2 q_0) \tag{A22}$$

with $\Delta v_0 = v_H - v_1$.

Full step, A: $\{q_0, v_H\} \Rightarrow \{q_1, w_H\}$ with $\theta = h$

$$\frac{dq}{dt} = v \quad \Rightarrow \quad q_1 = \cos(\theta)\, q_0 + \sin(\theta)\, v_H \tag{A23}$$

$$\frac{dv}{dt} = -q \quad \Rightarrow \quad w_H = -\sin(\theta)\, q_0 + \cos(\theta)\, v_H \tag{A24}$$

half step, B: $\{q_1, w_H\} \Rightarrow \{q_1, v_1\}$ with $M = (L + A_{ou}^2\mathbb{1})$

$$M\frac{dv}{dt} = -(\phi(q) - A_{ou}^2 q) \;\Rightarrow M\Delta v_1 = -\frac{h}{2}(\phi(q_1) - A_{ou}^2 q_1) \tag{A25}$$

with $\Delta v_1 = v_1 - w_H$.

Appendix D. BAB Splitting: Energy Error

When using the BAB splitting, the error in the effective energy is

$$\begin{aligned} \Delta E^{(01)} \quad &= \Phi(q_1) - \Phi(q_0) - \frac{1}{2}\langle q_1 | A_{ou}^2 | q_1\rangle + \frac{1}{2}\langle q_1 | A_{ou}^2 | q_0\rangle \\ &+ \frac{1}{2}\langle v_1 | M | v1\rangle - \frac{1}{2}\langle v_0 | M | v_0\rangle + \frac{1}{2}\langle q_1 | M | q1\rangle - \frac{1}{2}\langle q_0 | M | q_0\rangle \end{aligned} \tag{A26}$$

which simplifies to

$$\begin{aligned} \Delta E^{(01)} \quad &= \Phi(q_1) - \Phi(q_0) - \frac{1}{2}\langle q_1 + q_0 | A_{ou}^2 | q_1 - q_0\rangle \\ &+ \frac{1}{2}\langle v_1 + w_H | M | v_1 - w_h\rangle + \frac{1}{2}\langle v_H + v_0 | M | v_H - v_0\rangle . \end{aligned} \tag{A27}$$

 doi:10.20944/preprints202103.0608.v1

One can express this in terms of q_0 and q_1, using equations A22, A25 and

$$v_H = -q_0 \cot\theta + q_1 \csc\theta \tag{A28}$$
$$w_H = \ q_1 \cot\theta - q_0 \csc\theta \tag{A29}$$

In the work by Beskos et al.[3], a similar method was constructed for the case where $A_{ou} = 0$. In the middle step of the numerical integration (full step A), the Crank-Nicolson method was used. This changes the rotation angle in equations A23 and A24 to be $\theta = \sin^{-1}\left(4h/(4+h^2)\right)$. This in turn modifies the solutions for v_H and w_H used in Beskos et al., namely

$$v_H = \frac{1}{h}(q_1 - q_0) + \frac{h}{4}(q_1 + q_0) \tag{A30}$$
$$w_H = \frac{1}{h}(q_1 - q_0) - \frac{h}{4}(q_1 + q_0) \tag{A31}$$

References

1. Englander, S.W.; Mayne, L. The case for defined protein folding pathways. *Proceedings of the National Academy of Sciences* **2017**, *114*, 8253–8258.
2. Onsager, L.; Machlup, S. Fluctuations and irreversible processes. *Physical Review* **1953**, *91*, 1505.
3. Beskos, A.; Pinski, F.; Sanz-Serna, J.; Stuart, A. Hybrid Monte Carlo on Hilbert spaces. *Stochastic Processes and their Applications* **2011**, *121*, 2201–2230.
4. Duane, S.; Kennedy, A.; Pendleton, B.J.; Roweth, D. Hybrid Monte Carlo. *Physics Letters B* **1987**, *195*, 216 – 222.
5. Neal, R.M. In *Handbook of Markov Chain Monte Carlo*; Brooks, S.; Gelman, A.; Jones, G.; Meng, X., Eds.; Chapman & Hall, CRC Handbooks of Modern Statistical Methods, Taylor & Francis, 2011; chapter 5, pp. 113–162.
6. Uhlenbeck, G.E.; Ornstein, L.S. On the Theory of the Brownian Motion. *Phys. Rev.* **1930**, *36*, 823–841.
7. Malsom, P.J.; Pinski, F.J. Role of Ito's lemma in sampling pinned diffusion paths in the continuous-time limit. *Phys. Rev. E* **2016**, *94*, 042131.
8. Malsom, P. Rare Events and the Thermodynamic Action. PhD thesis, University of Cincinnati, 2015.
9. Trotter, H.F. On the product of semi-groups of operators. *Proceedings of the American Mathematical Society* **1959**, *10*, 545–551.
10. Strang, G. On the construction and comparison of difference schemes. *SIAM journal on numerical analysis* **1968**, *5*, 506–517.
11. Rowlands, G. A numerical algorithm for Hamiltonian systems. *Journal of Comp. Phys.* **1991**, *97*, 235–239.
12. Toxvaerd, S. Hamiltonians for discrete dynamics. *Physical Review E* **1994**, *50*, 2271.
13. Øksendal, B. *Stochastic Differential Equations*; Universitext, Springer Berlin Heidelberg: Berlin, Heidelberg, 2003.
14. Stuart, A.; Voss, J.; Wiberg, P. Conditional Path Sampling of SDEs And The Langevin MCMC Method. *Comm. Math. Sci.* **2004**, *2*, 685.
15. Korol, R.; Rosa-Raíces, J.L.; Bou-Rabee, N.; Miller III, T.F. Dimension-free path-integral molecular dynamics without preconditioning. *The Journal of Chemical Physics* **2020**, *152*, 104102.
16. Pinski, F.J.; Stuart, A.M. Transition paths in molecules at finite temperature. *The Journal of Chemical Physics* **2010**, *132*, 184104.
17. Leimkuhler, B.; Matthews, C. Efficient molecular dynamics using geodesic integration and solvent–solute splitting. *Proceedings of the Royal Society A: Mathematical, Physical and Engineering Sciences* **2016**, *472*, 20160138.
18. Ottobre, M.; Pillai, N.S.; Pinski, F.J.; Stuart, A.M.; others. A function space HMC algorithm with second order Langevin diffusion limit. *Bernoulli* **2016**, *22*, 60–106.
19. Lavenda, B. Thermodynamic criteria governing the stability of fluctuating paths in the limit of small thermal fluctuations: critical paths in the limit of small thermal fluctuations: critical paths and temporal bifurcations. *Journal of Physics A: Mathematical and General* **1984**, *17*, 3353.
20. Maruyama, G. Continuous Markov processes and stochastic equations. *Rendiconti del Circolo Matematico di Palermo* **1955**, *4*, 48–90.

 doi:10.20944/preprints202103.0608.v1

21. Barczy, M.; Kern, P. Sample path deviations of the Wiener and the Ornstein–Uhlenbeck process from its bridges. *Brazilian Journal of Probability and Statistics* **2013**, *27*, 437–466.